

Roadside air pollution and secondary organic aerosol seasonal trends from an oxidation flow reactor in Seoul



Gyutae Park ^a, Seokwon Kang ^b, Min-Suk Bae ^c, Yunsung Lim ^d, Chan-Soo Jeon ^e, Taehyoung Lee ^{b,*}

^a Air Pollution Engineering Division, Climate and Air Quality Research Department, National Institute of Environmental Research, Incheon, 22689, Republic of Korea

^b Department of Environmental Science, Hankuk University of Foreign Studies, Yongin, 17035, Republic of Korea

^c Department of Environmental Engineering, Mokpo National University, Muan, 58554, Republic of Korea

^d Transportation Pollution Research Center, National Institute of Environmental Research, Incheon, 22689, Republic of Korea

^e Korea Institute of Civil Engineering and Building Technology, Goyang, 10223, Republic of Korea

HIGHLIGHTS

- The seasonal study in South Korea about air pollution and secondary aerosol using an oxidation flow reactor.
- The characteristics of pollutants are different according to the composition of traffic volume by fuel types.
- Spring, Summer, and Fall exhibited more SOA products than winter under various OH· concentration.
- The IVOCs were the key group of the SOA compared to that formed from anthropogenic VOCs, SVOCs, and BVOCs.

ARTICLE INFO

Keywords:

Oxidation flow reactor (OFR)
Secondary organic aerosol (SOA)
Korean holidays
Roadside air pollutants
Seoul

ABSTRACT

The aim of this study was to determine the seasonal trends in secondary aerosols (SAs) and urban pollutants formed in an oxidation flow reactor (OFR) at a key roadside location in Seoul, South Korea. Spring 2019 saw high primary concentrations overall, and all seasons saw high levels of NO_x, SO₂, and equivalent black carbon (eBC) trends in the early morning (6:00–7:00). This exhibited similarities to the trend in diesel vehicle traffic volume. During the campaign, the modified hydroxyl radical (OH) exposure in the OFR was $\sim 1.1 \times 10^{12}$ molecules cm⁻³ s (~ 8.5 days), and the potential organic aerosol enhancement (OA_{PE}) was 0.4–57.7 $\mu\text{g m}^{-3}$ (winter 0.4–1.6, spring 28.4–52.3, summer 40.5–57.7, fall 18.1–31.1). The highest OA_{PE}/ΔCO value was 89.5–414.7 $\mu\text{g m}^{-3}$ for 0.1–4 OH-day in summer, and the lowest level was 1.1–8 $\mu\text{g m}^{-3}$ for 0.5–8.5 in OH-day winter (including holidays). OA_{PE} in seasons without winter under ~ 4.5 OH· day had a ~ 5.5 times higher value compared to that of organic on the roadside, accounting for 50.9–70.2% of the total sum (organic + eBC + OA_{PE}). This had a high contribution to secondary organic aerosol (SOA) formation and, for winter, a value of only $\sim 5.5\%$. The predicted SOA formation from intermediate volatile organic compounds (IVOCs) calculated based on literature was 11–47% during mornings (9:30–11:30), excluding the winter season. This value was higher than the SOA formation from anthropogenic VOCs (benzene, toluene, ethylbenzene, and *m,p,o*-xylene) and biogenic VOCs (isoprene, monoterpenes, and sesquiterpenes), indicating the need for additional research into the domestic status of IVOCs. The marked seasonal change in South Korea's climate made applying research findings from other countries difficult. Therefore, further studies must be conducted based on realistic applicability, considering various environmental conditions, chemical speciation, and the classification of emission inventory components.

* Corresponding author.

E-mail address: thlee@hufs.ac.kr (T. Lee).

1. Introduction

Internal combustion engine (ICE) vehicles powered by fossil fuels have become a popular mode of transportation, providing the general public with more convenience. However, air pollutants emitted by these vehicles are the primary source of urban air pollution and potential global warming, posing a socioeconomic challenge for modern society (Liu et al., 2020; Zhou et al., 2020). As the use of motor vehicles is closely associated with public life, short- and long-term exposure to pollutants from motor vehicle emissions harms human health in a variety of ways, including cardiovascular disease, pulmonary function decline, cancer, and mortality (Brugge et al., 2007; Sydbom et al., 2001; Wichmann, 2007).

Primary pollutants emitted by motor vehicles include carbon monoxide (CO), non-methane organic gas (NMOG), nitrogen oxides (NO_x), sulfur dioxide (SO_2), and particulate matter (PM) (Pieber et al., 2018; Roth et al., 2020). However, a few substances produce secondary aerosols (SAs), secondary air pollutants, through a radical chemical reaction with other atmospheric components (Karjalainen et al., 2019; Simonen et al., 2019).

Metropolitan cities in South Korea have a high population density and, consequently, a concentrated motor vehicle distribution. According to Ministry of Land, Infrastructure, and Transport (MOLIT) statistics, the registered motor vehicles in the Seoul Metropolitan Area (Seoul, Gyeonggi, and Incheon) account for 47% (787,178 vehicles) of the total number of registered motor vehicles nationwide (1,657,691 vehicles). As a result, Seoul, a metropolitan city, has high levels of air pollution caused by motor vehicle emissions, with CO emissions from on-road vehicles accounting for 64% (36,116 tons), NO_x for 49% (37,515 tons), PM_{2.5} for 30% (503 tons), and NMOG for 11% (7492 tons) of total emissions (Ministry of Environment (MOE), 2017 National Air Pollutants Emission Report).

NMOG emission concentrations from motor vehicle exhaust are reduced after treatment with devices such as three-way catalysts (TWC) and diesel oxidation catalysts (DOC). However, with secondary air pollutant formation, NMOG has been frequently reported as the primary source of SOA formation in urban areas (Park et al., 2019; Shah et al., 2020; Saha et al., 2018a; Link et al., 2017). Moreover, recently, gasoline vehicles equipped with TWC generated NH₃ emissions as a by-product in the process of reducing pollutants, which led to atmospheric reactions with NO_x , thus contributing to the formation of ammonium nitrate (NH₄NO₃), a type of secondary inorganic aerosol (SIA) (Park et al., 2021a; Link et al., 2017; Suarez-bertoa et al., 2014).

Hence, to assess air pollution caused by motor vehicle emissions, it is necessary to investigate the primary emissions and secondary pollutant formation. Tkacik et al. (2014) used an oxidation flow reactor (OFR) in a tunnel located in a metropolitan area in the United States to study the formation of SA. As a result, SOA production was reported to be up to six times greater than the total aerosol emissions from on-road mobile sources in the United States. This indicates that motor vehicle emissions significantly contribute to the formation of SA in densely populated urban areas. Saha et al. (2018a) conducted research using an OFR in the summer and winter seasons near highways in North Carolina, reporting that seasonal temperature changes affected the volatility distribution and reaction activity of NMOGs. SOA formation increased during the summer, when temperatures were generally higher than in the winter. Through their research on SOA formation from Beijing and Hong Kong roadsides, Liao et al. (2021) and Liu et al. (2019) reported the importance of measuring precursor gases in motor vehicles, such as intermediate volatile organic compounds (IVOCs). The secondary particulate matter production factor was ~2.6 times higher than primary particle production [equivalent black carbon (eBC) + hydrocarbon-like organic aerosol (HOA)].

As described above, previous studies on SA formation have advantages in terms of a comprehensive and realistic evaluation of air pollution from motor vehicle emissions in the atmosphere. However, SA

research based on real-time measurements has not yet been conducted in South Korea. Therefore, this study comprehensively evaluated air pollutants from roadside motor vehicle emissions and SA formation in an OFR in South Korea. In this study, seasonal trends (spring, summer, fall, and winter) were measured from a roadside area that represents the traffic volume according to the vehicle fuel type distribution in Seoul. Furthermore, considering the traditional representative holidays in South Korea, Korean New Year (KNY) and Korean Thanksgiving Day (KTD) on the lunar calendar, the days of measurements were classified into normal days and holidays (KNY, KTD) to investigate the changes in traffic by fuel type. Thus, a comparative analysis of various types of pollutants and characteristics of SA formation was performed. This study's findings contribute substantially by presenting an analysis of the formation of secondary pollutants and the investigation of primary air pollutants from motor vehicle emissions, which has been the primary focus of previous studies, thus facilitating a comprehensive evaluation and understanding of the status of air pollution from motor vehicle emissions.

2. Methodology

2.1. Location

In this study, a simplified measurement station was installed below the management office outside the Hongjimum Tunnel in Seoul in 2019. Measurements were taken for up to 13 days in the winter (January), spring (April), summer (July), and fall (September) (more information can be obtained in Supporting information SI, Table S1). This area has an average round-trip traffic volume of 160,768 vehicles day⁻¹, according to the average traffic volume statistics in downtown Seoul in 2016. Measurements were conducted in the Kookmin university-direction lane, in which the average traffic volume is approximately 75,000 vehicles day⁻¹ on weekends and approximately 80,000 vehicles day⁻¹ on weekdays. Additionally, it is advantageous for the intensive measurement of air pollutants from motor vehicle emissions because the area's curved terrain is less affected by pollutant inflow from outside sources. During the study period, the temperature was $-3.9 \pm 4.9^\circ\text{C}$ in the winter, $14.1 \pm 4.7^\circ\text{C}$ in the spring, $24.8 \pm 3.3^\circ\text{C}$ in the summer, and $23 \pm 3.3^\circ\text{C}$ in the fall. The relative humidity was $47.3 \pm 17.5\%$ in the winter, $67.5 \pm 21.6\%$ in the spring, $67.7 \pm 15.7\%$ in the summer, and $64.3 \pm 20.2\%$ in the fall. As for the traditional representative holiday periods in South Korea, KNY was set from 00:00 on February 2nd to 00:00 on February 7th. KTD was set from 00:00 on September 12th to 00:00 on September 15th (SI, Table S1). In this study, the winter and spring measurements were conducted concurrently with another project in the same location; therefore, some of the traffic environment data (traffic volume by fuel type) included in the results were obtained by Park et al. (2021b); otherwise, the other data was not duplicated in any way.

2.2. Instrument setup

During the setup, roadside pollutants were introduced into the simplified measurement station using a blower from a duct at 4 m from the lane and 1.5 m from the ground to perform isokinetic sampling. Gas-phase components including CO (Serinus 30, Ecotech), NO_x (NO, NO₂) (42C, Thermo Scientific), SO_2 (43C, Thermo Scientific), O₃ (49C, Thermo Scientific), and CO₂ (LI-840, LI-COR) were measured. The NH₃ (EAA-911, Los Gatos Research) sampling line was heated in the summer and fall due to the air conditioner operation to maintain the internal temperature (Kim et al., 2021). For the particle phase, eBC was measured using an aethalometer (AE33, Magee Scientific). A high-resolution time-of-flight aerosol mass spectrometer (HR-ToF-AMS, hereafter referred to as AMS, Aerodyne Research, Inc.) was used to determine the concentration of organic, nitrate, sulfate, ammonium, and chloride among PM₁ (Kang et al., 2020; Drewnick et al., 2005; DeCarlo

et al., 2006). The measurement using AMS was performed in V-mode at 1-min intervals, and data processing was performed in Igor Pro (version 8.04) using toolkits SQUIRREL (version 1.65) and PIKA (version 1.25), respectively. In this study, constant values of the relative ionization efficiency (RIE) were used with organic at 1.4, nitrate at 1.1, sulfate at 1.2, ammonium at 4, and chloride at 1.4 (Jimenez et al., 2003). For the collection efficiency (CE), through a comparison with the scanning mobility particle sizer (SMPS, model 3090, TSI), the default value of 1 was applied for the winter, spring, and summer seasons. Composition-dependent CE (avg. 0.65 ± 0.21) was applied for the fall season (Middlebrook et al., 2012, SI Fig. S1). Thereafter, CO_2 was measured from the front end of the AMS. Gaseous CO_2^+ was subtracted from organic (m/z 44) (Collier and Zhang, 2013). To reduce the effect of moisture, the sample was dried at constant humidity with a Nafion dryer (MD-110-24S-4, Perma Pure). For the traffic environment, an HD Digital Wave Radar (Smart Sensor HD Model 126, Wavetronix, Provo, UT, USA) was installed for real-time measurement of the total traffic and driving speed. The traffic volume depending on the fuel types of gasoline, LPG, and diesel vehicles was calculated using the statistical extraction method proposed by Park et al. (2021b). This study assumed that gasoline was used for passenger cars, diesel was used for sport utility vehicles (SUVs) and trucks, and LPG was used for taxis.

2.3. Oxidation flow reactor (OFR)

In a roadside atmosphere, changes in SA components were observed with different levels of exposure to hydroxyl radicals (OH) using an oxidation flow reactor (OFR). The OFR used in this study was first introduced by Kang et al. (2007) under the name of potential aerosol mass (PAM), and PAM was later commercialized by Aerodyne Research Inc. The OFR volume is 0.0133 m^3 (13.3 l); it is made of cylindrical aluminum and is coated with alodine to minimize corrosion and conductivity by particles. Other essential information regarding OFR can be obtained from previous studies (Lambe et al., 2011; Liu et al., 2021; Park et al., 2021a; Peng and Jimenez, 2020). To produce OH inside OFR, various levels of OH exposure were simulated by adjusting the lamp power ranging from 17 to 50% using the OFR185 method (two lamps) in which 185 and 254 nm were simultaneously irradiated from one UV radiation lamp (Rowe et al., 2020). The OFR was operated using an auto valve at 10-min intervals before and after the OFR. In this case, the concentration before the OFR was represented by the roadside air pollutants. For modeling OH exposure, a MATLAB-based photochemical model (<https://pamusersmanual.jimdofree.com>) was used. The input values of the inflowing gases NO, NO_2 , CO, and SO_2 , and temperature and RH, were used at an OFR inflow flow rate of 8.5 lpm with an average residence time of 94s. To validate the simulated OH exposure results, the model-provided O_3 concentration after OFR and the actual measured O_3 concentration after OFR (106-L, 2 B Technologies) were compared (SI Fig. S2). Thus, the maximum OH exposure in this study was $\sim 1.1 \times 10^{12}$ molecules $\text{cm}^{-3} \text{ s}$. When this value was converted using the daily OH exposure of 1.5×10^6 molecules cm^{-3} reported by Mao et al. (2009), the result was ~ 8.5 days. Furthermore, dark OFR (0% lamp power) was performed to compensate for particle loss and correct the aerosol concentration passing through the OFR (SI Fig. S3).

2.4. Morning hour (9:30–11:30) SOA estimation

In this study, SOA prediction by major NMOG component groups measured in the morning (9:30–11:30), mass closure with SOA measured after OFR, and comparative analysis of the cause were conducted. Recently, semi-volatile organic compounds (SVOCs) and IVOCs have been reported as groups of components that significantly contribute to the formation of atmospheric SOA, showing high SOA yields despite their trace amounts among motor vehicle emissions (Jathar et al., 2011, 2013; Ma et al., 2018; Robinson et al., 2007; Zhao et al. 2017, 2018). Therefore, SOA production and contribution were

estimated using the reported results for SVOCs and IVOCs in motor vehicles. In addition, the benzene, toluene, ethylbenzene, m + p-xylene, and o-xylene results (the representative components of anthropogenic VOCs [AVOC]) were used to calculate anthropogenic SOA (ASOA) (SI Section S1, Fig. S4, and Table S2). In addition, the isoprene, monoterpenes (α , β -pinene), and sesquiterpene (longifolene) results (the components of biogenic VOCs [BVOCs] measured using proton transfer reaction mass spectrometry [PTR-MS, Ionicon] during fall) were used to calculate seasonal biogenic SOA (BSOA) and the concentrations for the other seasons by applying equations S1–S3 described in SI section S1.

Equation (1) shows the calculation formula used in this study, as follows:

$$\text{SOA prediction} = [\text{VOCs}_{i(\text{antropo},\text{bio},\text{S}/\text{IVOCs})}] \times (1 - e^{-k_{\text{OH},i} \times [\text{OH}] \times \Delta t}) \times Y_i \quad (1)$$

VOCs_i denotes AVOC, BVOC, and S/IVOC (in the unit of $\mu\text{g m}^{-3}$), k_{OH} indicates OH reaction rate constant (25°C , molecules cm^{-3}), and $[\text{OH}] \times \Delta t$ is the OH exposure inside OFR. Y_i is the SOA yield of each component. In this study, values under high NO_x conditions were used (SI section, S1 Table S4). The SOA ($\mu\text{g m}^{-3}$) of IVOCs for gasoline and diesel vehicles was calculated using the IVOCs-to-HOA (SI section Table S3) approach reported by Shah et al. (2020). However, in this study an 8.5 ± 3.9 value was used for gasoline vehicles, which is the result under the hot start condition reported by Zhao et al. (2016). A 12.5 ± 3.6 value was used for diesel vehicles with installed after-treatment devices, including DPF. For SOA of SVOCs from diesel vehicles, the specific gravity value of volatility distribution among vehicles mounted with after-treatment devices, including DPF, was used, as reported by Zhao et al. (2015). The measured specific gravity value containing SVOCs was applied to the filter results in May et al. (2013) for gasoline vehicles.

3. Results and discussion

3.1. Seasonal roadside air pollutants

Fig. 1 depicts the seasonal distribution of air pollutant concentrations and traffic composition data for the entire measurement period. As shown in Fig. 1h, the seasonal average traffic volume in the winter, spring, summer, and fall was $67,279 (\pm 6,683)$, $72,966 (\pm 1,975)$, $70,028 (\pm 3,232)$, and $66,949 (\pm 5,554)$ vehicles day^{-1} , respectively, indicating no significant difference in the seasonal traffic volume distribution. During the seasonal measurements, the traffic volume and percentage for each fuel type were $31,950$ – $36,901$ vehicles day^{-1} for gasoline vehicles (accounting for 43–54%), $25,868$ – $33,212$ vehicles day^{-1} for diesel vehicles (accounting for 36–46%), and 4510 – 5102 vehicles day^{-1} for LPG vehicles (accounting for 9–11%) (SI Table S1). This finding is consistent with the vehicle occupancy ratios of the major fuel types reported in South Korea and Seoul in 2019 (Park et al., 2021a; SI Table S5). Therefore, the findings of this study represent the characteristics of motor vehicle pollutant emissions from various fuel types in the city center area. The average speed during the period for each season was $69.2 (\pm 11.9) \text{ km h}^{-1}$ for winter, $69.3 (\pm 1.4) \text{ km h}^{-1}$ for spring, $64.8 (\pm 6.9) \text{ km h}^{-1}$ for summer, and $63.9 (\pm 7.2) \text{ km h}^{-1}$ for fall, respectively.

The results for average CO, CO_2 , NO_x , SO_2 , and eBC concentrations were highest in the spring, followed by winter, summer, and fall (SI Table S6). However, for the air pollutant monitoring stations in the city center adjacent area, most of the components apart from O_3 were high in the winter, which could be attributed to the burning of various combustion sources due to the cold weather and the impact of low atmospheric mixing layer height (MLH) (SI Table S6). Therefore, the measurement point in this study, where combustion in the ICE of motor vehicles is a dominant activity, may differ to a certain extent from that of an adjacent monitoring station that includes the result values of different emission sources. The seasonal average CO (Fig. 1a) was $1.49 (\pm 0.36) \text{ ppm}$ in the winter, $1.83 (\pm 0.63) \text{ ppm}$ in the spring, $1.26 (\pm 0.6)$

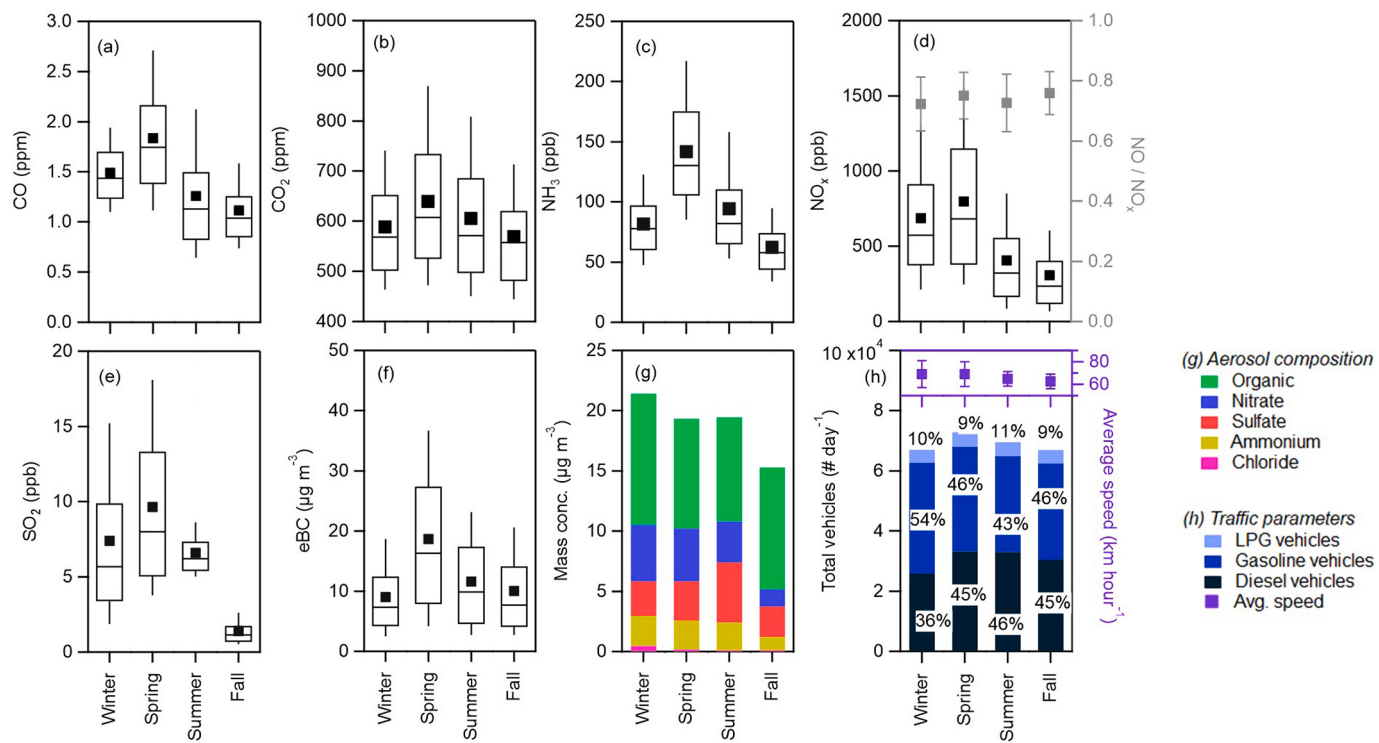


Fig. 1. Seasonal air pollution and traffic composition by fuel type on the roadside. (a–f) Show the box and whisker plots with the average value (dot) and median 75th, 25th, 90th, and 10th percentiles. (g) Chemical composition and aerosol concentration in PM₁. (h) Traffic distribution by fuel type (gasoline, diesel, and LPG) and average speed.

ppm in the summer, and 1.11 (± 0.38) ppm in the fall. The concentration of CO₂ (Fig. 1b), a greenhouse gas, was the highest in the spring at 630 (± 143) ppm, followed by 605 (± 143) ppm in the summer, 589 (± 112) ppm in the winter, and 569 (± 113) ppm in the fall. Turner et al. (2020) reported that urban anthropogenic CO₂ emissions decreased by 30% after COVID-19 compared to the values before the pandemic, with a 48% decrease in traffic accounting for the main cause. Therefore, with a concentrated distribution of mobile sources, motor vehicle emissions are the major source of anthropogenic CO₂ emissions in the city center. The SO₂ concentration (Fig. 1e) was 7.39 (± 5.66) ppb in the winter, 9.66 (± 5.71) ppb in the spring, 6.61 (± 1.64) ppb in the summer, and 1.41 (± 1.04) ppb in the fall, indicating that the value in the spring was the highest. The NO_x concentration was 686 (± 442) ppb in the winter, 798 (± 499) ppb in the spring, 407 (± 325) ppb in the summer, and 308 (± 267) ppb in the fall; thus, the values in the spring and winter were higher by 2.6 times than the values in the summer and fall. Grange et al. (2019) recently reported that NO_x emissions tend to increase with lower atmospheric temperatures (24.8–0.5 °C) and older diesel vehicles due to factors such as combustion activities and after-treatment device performance. In this study, the winter and spring with low temperatures showed a higher level of NO_x emissions than the summer and fall. As the main mobile source of NO_x emissions is diesel vehicles, it is critical to understand the effect of temperature changes on NO_x emissions in South Korea.

During the entire study period, O₃ was 3.45–9.63 ppb, nine times lower by season than the 16.8–35.2 ppb level at the monitoring station (SI Table S6). This significant difference is because O₃ was used in the NO oxidation process from motor vehicles to NO₂. Considering that NO/NO_x in Fig. 1d is 0.7–0.8, NO is still present in a significant portion of the roadside. Therefore, roadside-concentrated areas will likely increase NO₂ through atmospheric diffusion and oxidation processes in the surrounding atmosphere. Organic accounted for 25–42% during the seasonal measurement period, and eBC accounted for 29–47% of the total particle phase, accounting for most of the composition. The

percentage of organic in winter and fall was 37% and 42%, respectively, which are higher than that of eBC at 29% and 39%. During the spring and summer, eBC accounted for 47% and 40%, respectively, showing a higher percentage than organic at 25% and 30%. The nitrate concentration was 1.4–4.7 $\mu\text{g m}^{-3}$ (5–15%), and the sulfate concentration was 2.5–5 $\mu\text{g m}^{-3}$ (9–10%), consistent with the general level reported in the urban city center (Zhou et al. 2019a; Kim et al., 2018; Zhou et al. 2019a, 2020). However, due to the high concentration of eBC, the proportion of total particle phase was low, indicating that the measurement point in this study is directly affected by the primary pollutants. According to Kim et al. (2018), the average aerosol concentration in the city center area of Seoul was 22.1 $\mu\text{g m}^{-3}$ during the Korea-US Air Quality Study (KORUS-AQ) conducted in the spring season from April 14th to May 15th, 2016. The average organic concentration was 9.76 (± 5.27) $\mu\text{g m}^{-3}$ (47%), nitrate was 3.78 (± 4.2) $\mu\text{g m}^{-3}$ (17%), sulfate was 4.4 (± 3.26) $\mu\text{g m}^{-3}$ (20%), and eBC was 1.52 (± 0.82) $\mu\text{g m}^{-3}$ (7%). Conversely, during the spring season of this study, the eBC concentration was 18.7 (± 12.31) $\mu\text{g m}^{-3}$, accounting for 47%. The concentrations of other components were like the values reported by Kim et al. (2018).

NH₃ emissions from motor vehicles are typically a by-product of air pollutant reduction using TWC, which are after-treatment devices for gasoline and LPG vehicles (Park et al., 2019; Suarez-Bertoá et al., 2014; Wang et al., 2019a). Moreover, NH₃ emissions from gasoline vehicles are known to have a high correlation with CO. Fig. S5 shows a seasonal comparison of NH₃ and CO (Suarez-Bertoá et al., 2014; Walters et al., 2020; Park et al., 2023). The Pearson correlation coefficients (*r*) for spring, summer, and fall were 0.724, 0.824, and 0.834, respectively, showing a high linear correlation and 0.266 for the winter. In the winter, high-temperature exhaust gases, including NH₃, are emitted under low-temperature conditions, and the concentration is low due to condensation and gas-particle partitioning (Chang et al., 2016; Wang et al., 2019b).

3.2. Seasonal diurnal variations, including Korean New Year and thanksgiving holiday

Fig. 2 depicts the diurnal pattern by season and the comparison results between KNY and KTD, the longest holidays in Korea. For changes in concentration by season during routine periods (excluding holidays), CO in Fig. 2a describes the first rising curve regarding the increase in total traffic volume from 04:00 or 05:00 to 21:00 and the second rising curve from 21:00 to 04:00 the following day. The characteristics of the first rising curve are thought to be the effect of the CO inflow to the sampling tube in the low level of the diluted state in the vertical and horizontal directions due to the continuous traffic volume (seasonal 3182 ± 149 vehicles h^{-1}) and average speed (65.3 ± 2.9 km h^{-1}) despite the increase in air temperature from sunlight during the daytime and rising mixing layer height (MLH). The second rising curve was the effect of LPG vehicle traffic volume changes and the rising proportion of LPG and gasoline vehicles (~77%), as shown in Fig. S6d. As most of the gas-phase components of motor vehicle pollutants are emitted as CO_2 , the hourly pattern of CO_2 in this study showed a seasonal trend like that of traffic volume (Mitchell et al., 2018; Zhang et al., 2018). For NH_3 , during the summer, fall, and spring, the concentration increased from 05:00, the time when the traffic volume started to increase. By season, peaks of 99 ppb in the winter, 208 ppb in the spring, 147 ppb in the summer, and 96 ppb in the fall were observed at 17:00. After 17:00 for

the spring, summer, and fall, NH_3 decreased until 05:00; however, in the winter, the NH_3 concentration increased from 23:00 and reached its second peak at 02:00. The difference in the maximum and minimum values of each peak was $\Delta 116$ ppb in the spring, $\Delta 96$ ppb in the summer, $\Delta 62$ ppb in the fall, and $\Delta 47$ ppb in the winter. The reason for the considerable difference in NH_3 variation despite similar traffic volume is thought to be associated with the ammonia partitioning under low air temperature and reaction temperature of the TWC, along with the explanation provided in 3.1 (Zhou et al., 2019b; Żółtowski and Gis, 2021).

In this study, NO_x , SO_2 , and eBC exhibited clear similarities to traffic patterns of diesel vehicles during the peaks in the hours of 6:00–7:00, as shown in SI Fig. S6c. During these hours, the diesel vehicles outnumbered gasoline vehicles by 1.8 times, accounting for 49–60% of the total traffic. After this hours, the proportion of diesel vehicles decreased. Concurrently, the concentration of air pollutants decreased. The values began to rise again at 09:00. Park et al. (2019) reported that from investigating the gaseous emissions from motor vehicles by fuel type, among the components of the gaseous emissions from diesel vehicles excluding CO_2 , the emissions of NO_x and SO_2 accounted for ~91.2% and ~0.63%, respectively. However, gasoline and LPG vehicles accounted for ~1.4% of NO_x and ~0.03% of SO_2 emissions, indicating that these two vehicles have a low level of contribution by vehicle fuel type. In this study, the changes in the proportion of traffic volume for diesel vehicles,

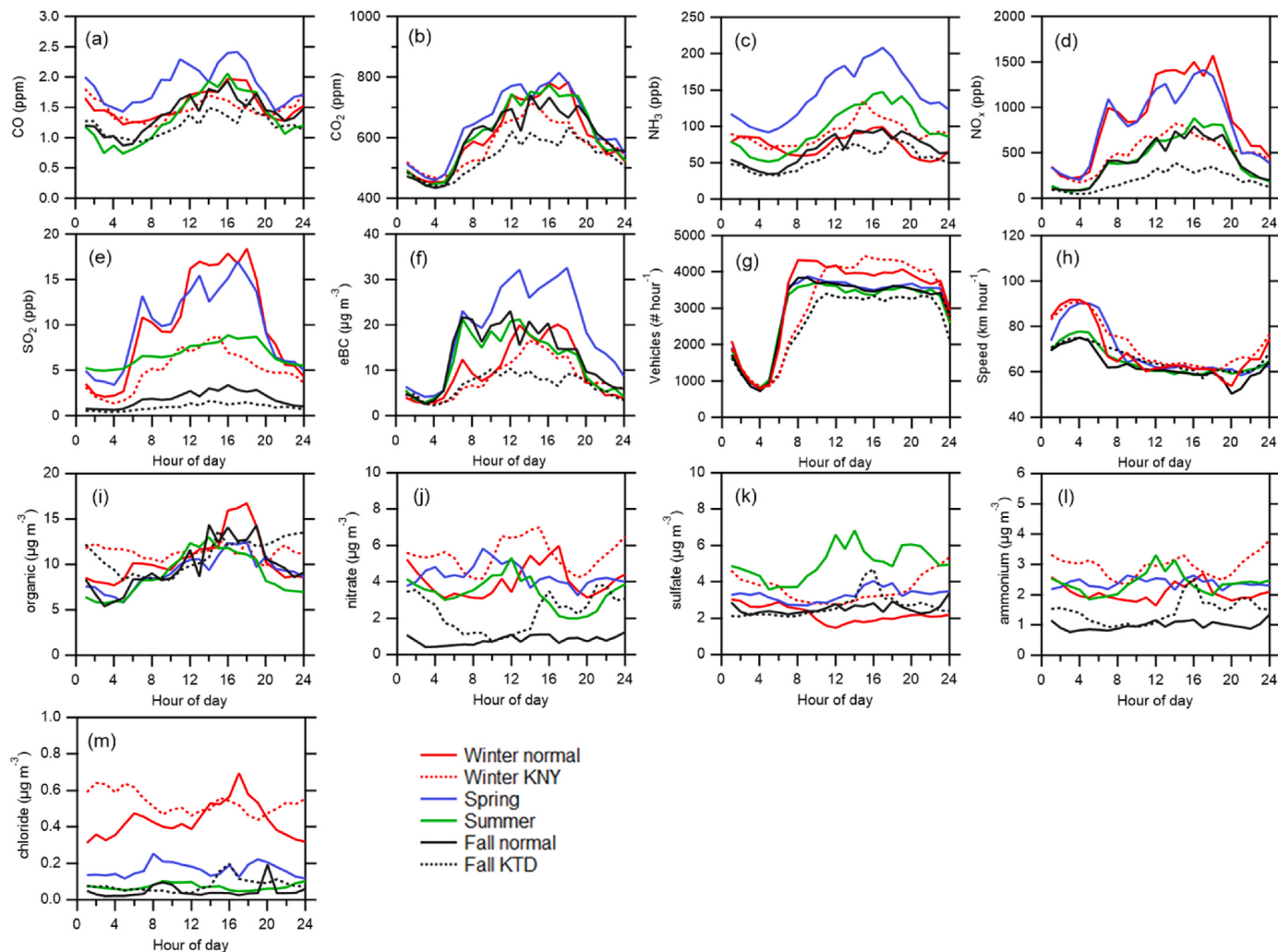


Fig. 2. Diurnal variation of gases (CO , CO_2 , NH_3 , NO_x , SO_2), eBC, traffic condition (total number of vehicles per hour and average speed), and aerosols (organic, nitrate, sulfate, ammonium, and chloride) in the seasonal campaign. The thick lines refer to a normal period, and the dotted lines occurred during Korean New Year (KNY, red) and Korean Thanksgiving Day (KTD, black).

and NO_x concentration, and SO_2 showed a similar trend. For O_3 (Fig. S6a), due to the high NO concentration, regardless of the season, the concentration of O_3 was deficient, with an average of $4.6 (\pm 3.0)$ ppb when the proportion of diesel vehicles was high in the traffic volume. As shown in Fig. 1d, as the portion of NO is still high, the ambient NO_2 concentration is expected to rise due to oxidation. For eBC (Fig. 2f), diesel vehicles are the most significant contributor to the first peak. The distribution of concentration after the first peak with the increase in traffic volume was mainly affected by the combined effect of gasoline and diesel vehicles. This is because diesel vehicle contributions to eBC emissions vary according to vehicle age. Additionally, there are contributions from gasoline vehicles equipped with direct injection (GDI) engines (Fushimi et al., 2016; Saliba et al., 2017). The concentration of eBC was higher in the summer than in the winter, with the same seasonal trend reported by Saha et al. (2018b) and Wang et al. (2018). In South Korea, eBC emissions may be high in the summer due to changes in fuel composition to satisfy gasoline's increased vapor pressure regulation. For example, Karavalakis et al., 2015 reported that as the aromatic content in gasoline increased, eBC emissions increased 1.54 times the aromatic content of 30% compared to the 15% content. Therefore, the eBC emissions on roadsides with a high proportion of gasoline vehicles should consider the effect of the seasonal fuel composition. The diurnal pattern of organic variation was similar to changes in traffic volume, and nitrate in the fall was the lowest concentration pattern in other seasons. During the summer, the sulfate concentration increased during the day and peaked at $6.8 \mu\text{g m}^{-3}$ between 13:00 and 14:00. The reason was that the sulfur dioxide photochemical oxidation process and the attribution to aqueous phase reaction in wet aerosols due to the higher temperature and humidity than in other seasons (Hu et al., 2017). The pattern of ammonium was followed by nitrate and sulfate because they primarily exist in the forms of ammonium sulfate $(\text{NH}_4)_2\text{SO}_4$ and NH_4NO_3 . In the case of chloride, the variation in concentration over time was insignificant. However, in winter, the chloride was higher than in other seasons due to the high background level of the source of coal combustion surrounding the roadside.

The comparison results for gas- and particle-phase pollutants between the major holiday periods (KNY in the winter and KTD in the fall) and the routine traffic environment are summarized in the dotted line illustrated in Fig. 2 and S6–7. Compared to the normal period, the traffic volume decreased by 15% during KNY and 14% during KTD; however, the percentage of gasoline vehicles increased from 48% to 59% during KNY and from 43% to 50% during KTD. The percentage of diesel vehicles decreased from 42% to 31% during KNY and from 47% to 40% during KTD compared to the normal period. The proportion of trucks in the traffic volume decreased from 0.3 to 0.11 (62%) during KNY and from 0.28 to 0.09 (67%) during KTD (SI Fig. S7b). During the holidays, the trends in gas- and particle-phase pollutants changed according to the representative pollutants, considering the traffic volume for each fuel type. A clear reduction in NO_x and SO_2 emissions was observed due to a decrease in diesel trucks. During holiday periods, the NO_x concentration decreased from $845.7 (\pm 510.1)$ ppb and $395.3 (\pm 304.7)$ ppb to $501.3 (\pm 239.7)$ ppb and $190.2 (\pm 134.8)$ ppb for KNY and KTD, respectively (Fig. 2d, SI Table S7). For SO_2 emissions, the concentration decreased from $9.5 (\pm 6.58)$ ppb and $1.8 (\pm 1.2)$ ppb to $4.97 (\pm 2.82)$ ppb and $0.9 (\pm 0.5)$ ppb for KNY and KTD, respectively (Fig. 2e, SI Table S7). Since the high displacement from trucks causes higher emissions than other vehicles, the percentage of trucks in the traffic volume is a key control category for NO_x and SO_2 emissions on urban roadsides. Likewise, the eBC emissions during holiday periods decreased from winter-normal $9.71 (\pm 7.17) \mu\text{g m}^{-3}$ and fall-normal $12.58 (\pm 9) \mu\text{g m}^{-3}$ to KNY $8.2 (\pm 5.34) \mu\text{g m}^{-3}$ and KTD $6.53 (\pm 3.62) \mu\text{g m}^{-3}$, which corresponds to a reduction of 16% and 48%, respectively. The eBC emissions are affected by the contribution from GDI-mounted gasoline vehicles, as described above; thus, it is difficult to define a single cause for the emissions. However, the percentage of trucks in traffic volume had a considerable impact. For organic and inorganic (nitrate, sulfate, ammonium, and

chloride) emissions, the concentration was 2–65% higher during holiday periods (SI Table S7). The aerosol composition was as follows: During the KNY period, eBC was 25% ($8.2 \mu\text{g m}^{-3}$), organic was 36% ($11.38 \mu\text{g m}^{-3}$), nitrate was 16% ($5.46 \mu\text{g m}^{-3}$), sulfate was 12% ($3.63 \mu\text{g m}^{-3}$), ammonium was 9% ($2.96 \mu\text{g m}^{-3}$), and chloride was 2% ($0.53 \mu\text{g m}^{-3}$). During the KTD period, eBC was 30% ($6.53 \mu\text{g m}^{-3}$), organic was 47% ($10.81 \mu\text{g m}^{-3}$), nitrate was 7% ($2.25 \mu\text{g m}^{-3}$), sulfate was 10% ($2.57 \mu\text{g m}^{-3}$), ammonium was 5% ($1.41 \mu\text{g m}^{-3}$), and chloride was 1% ($0.08 \mu\text{g m}^{-3}$). Moreover, the CO and CO_2 concentration decreased by 3% (1.51 ppm vs. 1.47 ppm) and 4% (600.2 ppm vs. 575.5 ppm) during KNY compared to the normal period, and by 15% (1.19 ppm vs. 1.01 ppm) and 11% (596.4 ppm vs. 531.5 ppm) during KTD. For NH_3 emissions, the concentration was higher during KNY with an average of $91 (\pm 31.3)$ ppb, a 17.7 ppb increase compared to winter-normal; however, during KTD, with an average of $54.8 (\pm 20)$ ppb, a 13.2 ppb decrease compared to $68 (\pm 29.9)$ ppb during fall-normal.

3.3. Seasonal SOA formation

Table S8 outlines the seasonal trend in the potential enhancement (PE) of organic and inorganic aerosol (nitrate, sulfate, ammonium, and chloride) emissions produced inside the OFR. Hereafter, organic PE is referred to as OA_{PE} and inorganic PE as species_i PE. In this study, PE accounted for aerosol loss corrections and defined them as values obtained by subtracting the roadside concentration from the concentration formed inside the OFR. During the seasonal campaign, the OA_{PE} was $0.4\text{--}58 \mu\text{g m}^{-3}$ on average, at a photochemical OH^- concentration (hereafter referred to as $\text{OH}^- \text{ d}$) of up to $\sim 8.5 \text{ d}$. The sulfate_{PE} value was $\sim 0.6 \mu\text{g m}^{-3}$ in Fig. S8, similar to the roadside research result obtained by Liao et al. (2021) and tunnel research by Tkacik et al. (2014). This is because of the low seasonal SO_2 concentration ranging from 1.4 to 9.7 ppb compared to the high emission levels of NO_x and NH_3 from motor vehicles. In Fig. S8, the nitrate_{PE} value was $0.4\text{--}291 \mu\text{g m}^{-3}$; this is most likely due to the reaction between NH_3 and HNO_3 with a seasonal average ranging from 70 to 1574 ppb and NH_3 ranging from 35 to 209 ppb. The value of nitrate_{PE} inside the OFR is based on the thermodynamic equilibrium with NH_3 during the major reactions of NO and NO_2 , which are $\text{NO} + \text{O}_3 \rightarrow \text{NO}_2 + \text{O}_2$ and $\text{NO}_2 + \text{OH} \rightarrow \text{HNO}_3$, respectively.

Fig. 3a shows the seasonal change in OA_{PE} and the major holiday periods according to the $\text{OH}^- \text{ d}$. The seasonal OA_{PE} level was in the order of summer, spring, fall, and winter. The lowest production value was shown during winter-normal at $0.4\text{--}1.5 \mu\text{g m}^{-3}$ with the $\text{OH}^- \text{ d}$ ranging from 0.5 to 8.5. This result was like that reported by Saha et al. (2018a). The enhancement value was $\sim 0.5\text{--}1 \mu\text{g m}^{-3}$ for the measurement conducted during the winter season in the near highway. These low levels are due to decreased VOC activity at low temperatures. Furthermore, due to the increase in particle partitioning of S/IVOCs, the organic concentration on the roadside increased, which led to a decrease in the vapors of the components related to SOA formation. During the winter season in this study, the OA_{PE} values were similar between KNY and winter-normal, indicating no significant correlation with the traffic volume change of gasoline and diesel vehicles. During the summer, the value of OA_{PE} increased to $57.7 \mu\text{g m}^{-3}$ during 3–4 $\text{OH}^- \text{ d}$ and decreased after reaching the peak. However, for the spring season, the value of OA_{PE} showed a continuous increase from 28.4 to $52.3 \mu\text{g m}^{-3}$ for $0.4\text{--}4 \text{ OH}^- \text{ d}$. The atmosphere during spring was considered to be in a mixed state of rich anthropogenic and biogenic precursors and motor vehicle emissions. During the normal fall period, the OA_{PE} value was $18.1\text{--}3.1 \mu\text{g m}^{-3}$ for $0.2\text{--}4.3 \text{ OH}^- \text{ d}$, higher by $5.9\text{--}13.8 \mu\text{g m}^{-3}$ compared to the level during KTD. Platt et al. (2017) and Park et al. (2021a) reported in their chassis dynamometer research that the OA_{PE} value was higher for gasoline vehicles than in diesel vehicles. Due to this research and the increase in gasoline vehicle traffic volume, the result values during KTD are expected to be higher. However, the results of this study showed the opposite trend, indicating that IVOC emissions from diesel vehicles have a more significant contribution to roadside SOA formation than light

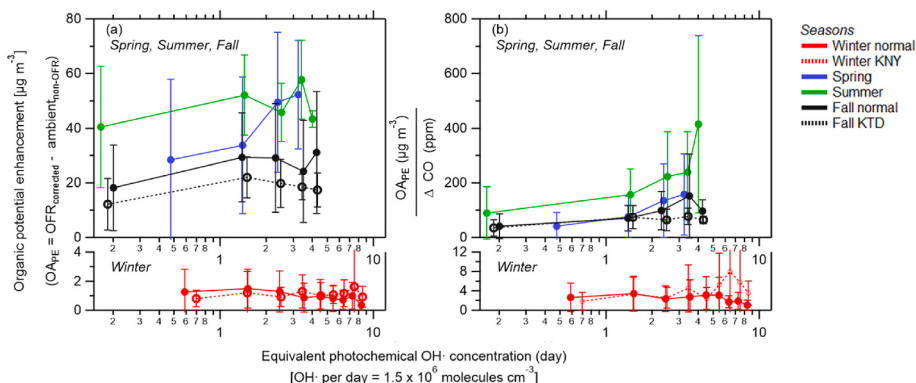


Fig. 3. (a) Seasonal organic potential enhancement (OA_{PE} = secondary organic aerosol formed and corrected in the oxidation flow reactor – organic corrected in the roadside) by increasing $OH\cdot$ concentration inside the OFR. (b) Ratio of $OA_{PE}/\Delta CO$ ($\mu g m^{-3} ppm^{-1}$) vs. $OH\cdot$ (ΔCO was subtracted from the background level of CO).

VOC emissions from gasoline vehicles (Lu et al., 2020; Zhao et al., 2015). Fig. S9 depicts the evolution of seasonal organics in a Van Krevelen diagram (Heald et al., 2010; Ng et al., 2011). The seasonal results of the roadside and roadside–normal showed that fitting the data yielded a slope of -0.79 to -0.9 , close to -1 , implying that the formation of carboxylic acid groups in our data is consistent. The SOA in winter fell along lines with a slope of -0.89 for winter-normal, and -0.87 for KNY. These were similar to the slopes of -0.9 for normal and -0.98 for KNY, indicating that the evolution of organic under $OH\cdot$ was followed by the same formation mechanism on the winter roadside conditions. In contrast, the slope of other seasons fell from -0.44 to -0.16 , indicating organic evolution chemistry involving an oxidation pathway between alcohol and/or peroxide and carboxylic acid functional groups without fragmentation in the presence of $OH\cdot$.

To demonstrate the trend in SOA formation according to urban combustion, the relation between the value of $OA_{PE}/\Delta CO$ ($\mu g m^{-3} ppm^{-1}$) and $OH\cdot d$ has been used in numerous previous studies (DeCarlo et al., 2010; Liu et al., 2019; Tkacik et al., 2014). The seasonal trend is illustrated in Fig. 3b. For ΔCO values, the value obtained by subtracting the background concentration was used, which is the method proposed by Gamage et al. (2020) (SI Fig. S10). During the spring and summer, the $OA_{PE}/\Delta CO$ values increased to $157.4 \mu g m^{-3} ppm^{-1}$ and $414.7 \mu g m^{-3} ppm^{-1}$, respectively, to the maximum $OH\cdot d$. However, after reaching peak values of $\sim 3.1 \mu g m^{-3} ppm^{-1}$ and $5.3 \mu g m^{-3} ppm^{-1}$ for ~ 4.5 and $5.5 OH\cdot d$, respectively, the values decreased during the winter-normal and KNY. Moreover, during the fall-normal and KTD, the values decreased after reaching the maximum values of $151.1 \mu g m^{-3} ppm^{-1}$ and $77.3 \mu g m^{-3} ppm^{-1}$ for ~ 3.5 and $3.4 OH\cdot d$, respectively. When the level of maximum values derived in this study was compared to the seasonal values obtained in overseas research, the winter values were higher by a factor of ~ 6 compared to $\sim 20 \mu g m^{-3} ppm^{-1}$ (10 m away from the highway and $6 \pm 7^\circ C$) as reported by Saha et al. (2018a), and lower by ~ 12 times compared to $\sim 382 \mu g m^{-3} ppm^{-1}$ ($18 \pm 3^\circ C$) as reported by Liu et al. (2019). For the spring, the value was higher by 1.7 times compared to $\sim 91 \mu g m^{-3} ppm^{-1}$ ($16^\circ C$), as reported in the tunnel research by Tkacik et al. (2014). For the summer, the value was seven times higher compared to $\sim 62 \mu g m^{-3} ppm^{-1}$ ($26 \pm 5^\circ C$) for $2-3 OH\cdot d$, as reported by Saha et al. (2018a). The trend in the change according to increasing $OH\cdot d$ in this study was like that of overseas studies. However, there were differences in the seasonal trend and the range of result values due to the following: First, even if overseas results were obtained in the same season as this study, there is a temperature effect due to the difference in actual seasonal temperatures by country. This is because temperature influences vehicle combustion efficiency and semi-volatile species gas-to-particle partitioning (Platt et al., 2017; Robinson et al., 2007). Second, there was a difference in the proportion of traffic volume by fuel type. As per the research of Saha et al. (2018a) and Tkacik et al. (2014), gasoline vehicles were the main fuel type, accounting for more

than 90%. However, research by Liu et al. (2019) had a mixed fuel type condition with gasoline at 40.8%, diesel at 30.3%, and LPG at 28.9%. For this study, the proportion of gasoline and diesel was higher, with gasoline at 46–54%, diesel at 36–46%, and LPG at 9–11%. Therefore, the VOC, IVOC, and SVOC emission levels vary depending on the fuel type contribution, and thus the consequent SOA formation level changes (Hu et al., 2022; Zhao et al., 2017; Zhao et al., 2016; Zhao et al., 2015).

3.4. Seasonal morning hour SOA estimation

Fig. 4 shows the SOA production estimation comparison calculated according to Section 2.4 and SI Section S1 from the organic and VOC groups formed inside the OFR during the morning (9:30–11:30). The total values of roadside organic, eBC, and OA_{PE} during the morning hours were $70.2 \pm 17.9 \mu g m^{-3}$, $67.9 \pm 28.5 \mu g m^{-3}$ for summer and spring, respectively, which are higher than the values of other seasons. During winter, the values were $25.5 \pm 7.0 \mu g m^{-3}$ during the normal period, $24.4 \pm 4.2 \mu g m^{-3}$ during KNY, and during fall, the values were $51 \pm 16.4 \mu g m^{-3}$ during the normal period, $32.1 \pm 8.3 \mu g m^{-3}$ during KTD. As for OA_{PE} , for $\sim 1 OH\cdot d$, the values were $\sim 41.8 \pm 11.2 \mu g m^{-3}$ during summer, $30.5 \pm 21.9 \mu g m^{-3}$ during spring, $20.1 \pm 13.3 \mu g m^{-3}$ during fall-normal, and $13.0 \pm 4.9 \mu g m^{-3}$ during KTD. During winter, for $\sim 5 OH\cdot d$, the values were $2.6 \pm 0.7 \mu g m^{-3}$ during winter-normal and $3.6 \pm 0.9 \mu g m^{-3}$ during KNY. In terms of total organic production estimated from the VOCs groups, the values were $27.7 \pm 7.3 \mu g m^{-3}$ during winter-normal and $15.1 \pm 2.5 \mu g m^{-3}$ during KNY. These result values are ~ 11 and ~ 4.2 times higher than the OA_{PE} result. In other seasons, the ratio of OA_{PE} to the estimated SOA production was 1.9–6.4, indicating that the estimated production was lower than the measured production. This underestimation trend was similarly observed in the results of the OFR vs. SOA estimation reported by Liao et al. (2021), Shah et al. (2020), and Saha et al. (2018a). For ASOA in winter, the values were $1.6 \mu g m^{-3}$ during normal winter and $1.2 \mu g m^{-3}$ during KNY, accounting for 62% and 33% of OA_{PE} , respectively. As for ASOA in spring, summer, and fall, the values were $\sim 1-4\%$. Thus, it is expected that the contribution of the major urban VOC components in the city center area to SOA formation in photochemical reactions is low. For S/IVOCs-SOA during the winter, the values were $25.9 \mu g m^{-3}$ during a normal winter and $13.7 \mu g m^{-3}$ during KNY, which are 10 times and 3.8 times larger than the value of OA_{PE} , which is thought to be due to the application of the S/IVOCs factor at room temperature. The reason is that S/IVOCs factors in this study are the result of chassis dynamometer test at $\sim 47^\circ C$ mixed exhaust with air, and S/IVOCs have a high proportion of gas-phase (Saha et al., 2018a; Zhao et al., 2016; Zhao et al., 2015). However, with a decrease in temperature, the evaporation of the component decreases, and the ratio of particle-phase increases. Therefore, at real-world low temperatures below zero due to the decrease in yield from reduced gas-phase S/IVOCs and low photochemistry activity,

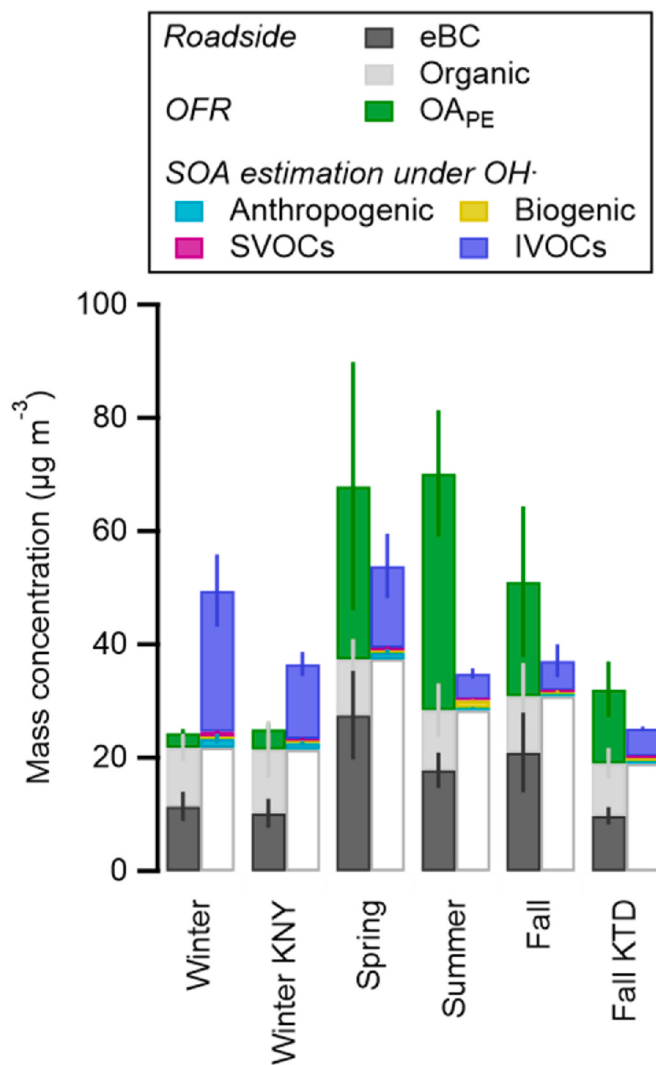


Fig. 4. Comparison of measured mass (eBC, organic, OA_{PE}) and SOA estimation under OH⁻ concentration during morning roadside hours (9:30–11:30) during each season. The first bars showed the sum of eBC, organic, OA_{PE}, and the white boxes in the second bars were the sum of eBC and organic, the same as the first bar's eBC and organic. The bars above the white boxes refer to the SOA estimation. The calculation of the SOA estimation for each VOC group was followed by Section 2.4, and the anthropogenic SOA was denoted for benzene, toluene, ethylbenzene, and (*m,p,o*-xylene. The biogenic SOA was calculated by tracking the fall results using PTR-MS. Additional information was discussed in SI Section 1. The S/IVOCs applications used the relationship between HOA and gasoline and diesel vehicles (Shah et al., 2020; Zhao et al., 2016; Zhao et al., 2015; and May et al., 2013).

the actual value of S/IVOCs-SOA is expected to be smaller (Drozd et al., 2021; Huang et al., 2019; Saha et al., 2018a). As for BSOA, the value was 1.4 µg m⁻³ during the summer when the tree activity level was higher than in other seasons; however, it had a small proportion of 3% among OA_{PE} groups. Therefore, an SOA estimation approach is required based on emission component fitting to the tree varieties around the site. The seasonal values of S/IVOCs-SOA ranged from 11 to 49% of OA_{PE} (excluding winter). With the inclusion of ASOA and BSOA, there is a gap of 6.9–35.3 µg m⁻³. Thus, to improve the SOA estimation approach's accuracy, the expansion of precursors and the shifting contribution of the gas-to-particle partitioning of volatile species for temperature should be considered.

4. Conclusion

Through in situ measurements, we completed a case study in South Korea that discusses a comprehensive seasonal trend analysis for the chemical characteristics of roadside pollutants and SA. The study's findings provide useful scientific reference data for evaluating and reducing roadside pollutants and highlight the need for additional research on various roadside environments in urban areas. The main findings of this study are as follows: Most seasonal roadside pollutants in Seoul in 2019 showed the highest concentration levels during the spring, followed by winter, summer, and fall. Regardless of the season, the 6–7 a.m. NO_x, SO₂ peaks and eBC showed a distinct similarity to the diesel vehicle traffic volume pattern. The NH₃ concentration increased up to the seasonal maximum of ~208 ppb (spring), consistent with the increase traffic volume. Regarding correlation with CO (excluding the winter season), the value of Pearson's *r* ranged from 0.724 to 0.834, indicating a high linear correlation. Considering the result of Park et al. (2019, 2021a), in which the main fuel types for CO and NH₃ emissions were reported to be gasoline and LPG vehicles mounted with TWC, the NH₃ vs. CO approach described in this study is expected to be useful for the level of contribution evaluation for NH₃ from the roadside environment with a combination of fuel types. During the ~4.5 OH⁻ d condition, common throughout seasons, the peak OA_{PE} value was ~1.5 µg m⁻³ in the winter, significantly lower than the peak value of ~57.7 µg m⁻³ for the other seasons. The value of Δorganic/ΔCO (µg m⁻³ ppm⁻¹) was ~3.4 µg m⁻³ ppm⁻¹, which is lower than the summer season peak value of ~414.7 µg m⁻³ ppm⁻¹. OA_{PE} had a ~5.5 times higher value than roadside organic pollutants in other seasons, accounting for 50.9–70.2% of the total sum (organic + eBC + OA_{PE}) and only ~5.5% in winter (SI Table S9). Therefore, even with an increase in OH⁻ d, the contribution from primary emissions is greater than the SOA contribution from photochemical reactions during the winter season.

For the seasonal trend (excluding winter), IVOCs accounted for 11–47% SOA formation during the morning (9:30–11:30). Although the study was based on the findings of previous studies, more research on IVOCs is needed to understand and interpret SOA formation trends in South Korea. Finally, we would like to emphasize the following: The particulate matter filter after-treatment device reduced motor vehicle particulate matter emissions in South Korea to an unprecedented level. However, when it came to reducing gas phase pollutants, the focus was primarily on NO_x. Although the reduction of NO_x emissions from motor vehicles is critical, the findings of this study and the results of several overseas research highlight the importance of reducing NH₃ emissions from vehicles mounted with TWC and reducing S/IVOCs emissions among NMOGs regardless of fuel type to achieve a real reduction in SA formation. Thus, further research is needed to address the issues raised above and policy-backed reduction measures.

CRediT authorship contribution statement

Gyutae Park: Conceptualization, Methodology, Formal analysis, Investigation, Writing – original draft, review, editing. **Seokwon Kang:** Methodology, Formal analysis. **Min-Suk Bae:** Validation, of VOCs results, cooperation of the measurement site. **Yunsung Lim:** Formal analysis, installation sampling system. **Chan-Soo Jeon:** Resources, Investigation. **Taehyoung Lee:** Conceptualization, Project administration, Supervision, Writing – original draft.

Declaration of competing interest

The authors declare that they have no known competing financial interests or personal relationships that could have appeared to influence the work reported in this paper.

Data availability

No data was used for the research described in the article.

Acknowledgements

We thank the research scientists at the Transportation Pollution Research Center. This work was supported by a grant from the National Institute of Environment Research (NIER), funded by the Ministry of Environment (MOE) of the Republic of Korea (NIER-2019-04-02-018). The extended experiment was conducted by the Korea Basic Science Institute (National Research Facilities and Equipment Center) grant, funded by the Ministry of Education (2019R1A6C1020041). The views expressed in the research are solely the authors' views and do not necessarily reflect the MOE's view. Additional data processing was supported by NRF (National Research Foundation of Korea) and both Ministry of Science and ICT (2019M1A2A2103953) and (2020M3G1A1114997).

Appendix B. Supplementary data

Supplementary data to this article can be found online at <https://doi.org/10.1016/j.atmosenv.2023.120051>.

Appendix A. Supplementary material

Supplementary data to this article can be found online at.

References

- Brugge, D., Durant, J.L., Rioux, C., 2007. Near-highway pollutants in motor vehicle exhaust: a review of epidemiologic evidence of cardiac and pulmonary health risks. *Environ. Health* 6, 23. <https://doi.org/10.1186/1476-099X-6-23>.
- Chang, Y., Zou, Z., Deng, C., Huang, K., Collett, J.L., Lin, J., Zhuang, G., 2016. The importance of vehicle emissions as a source of atmospheric ammonia in the megacity of Shanghai. *Atmos. Chem. Phys.* 16, 3577–3594. <https://doi.org/10.5194/acp-16-3577-2016>.
- Collier, S., Zhang, Q., 2013. Gas-phase CO₂ subtraction for improved measurements of the organic aerosol mass concentration and oxidation degree by an aerosol mass spectrometer. *Environ. Sci. Technol.* 47, 14324–14331. <https://doi.org/10.1021/es404024h>.
- DeCarlo, P.F., Kimmel, J.R., Trimborn, A., Northway, M.J., Jayne, J.T., Aiken, A.C., Gonin, M., Fuhrer, K., Horvath, T., Docherty, K.S., Worsnop, D.R., Jimenez, J.L., 2006. Field-deployable, high-resolution, time-of-flight aerosol mass spectrometer. *Anal. Chem.* 78, 8281–8289. <https://doi.org/10.1021/ac061249n>.
- DeCarlo, P.F., Ulbrich, I.M., Crounse, J., de Foy, B., Dunlea, E.J., Aiken, A.C., Knapp, D., Weinheimer, A.J., Campos, T., Wennberg, P.O., Jimenez, J.L., 2010. Investigation of the sources and processing of organic aerosol over the Central Mexican Plateau from aircraft measurements during MILAGRO. *Atmos. Chem. Phys.* 10, 5257–5280. <https://doi.org/10.5194/acp-10-5257-2010>.
- Drewnick, F., Hines, S.S., DeCarlo, P., Jayne, J.T., Gonin, M., Fuhrer, K., Weimer, S., Jimenez, J.L., Demerjian, K.L., Borrmann, S., Worsnop, D.R., 2005. A New time-of-flight aerosol mass spectrometer (TOF-AMS)—instrument description and first field deployment. *Aerosol Sci. Technol.* 39, 637–658. <https://doi.org/10.1080/02786820500182040>.
- Drozd, G.T., Weber, R.J., Goldstein, A.H., 2021. Highly resolved composition during diesel evaporation with modeled ozone and secondary aerosol formation: insights into pollutant formation from evaporative intermediate volatility organic compound sources. *Environ. Sci. Technol.* 55, 5742–5751. <https://doi.org/10.1021/acs.est.0c08832>.
- Fushimi, A., Kondo, Y., Kobayashi, S., Fujitani, Y., Saitoh, K., Takami, A., Tanabe, K., 2016. Chemical composition and source of fine and nanoparticles from recent direct injection gasoline passenger cars: effects of fuel and ambient temperature. *Atmos. Environ.* 124, 77–84. <https://doi.org/10.1016/j.atmosenv.2015.11.017>.
- Gamage, L.P., Hix, E.G., Gichuhi, W.K., 2020. Ground-based atmospheric measurements of CO:CO₂ ratios in eastern highland rim using a CO tracer technique. *ACS Earth Space Chem.* 4, 558–571. <https://doi.org/10.1021/acsearthspacechem.9b00322>.
- Grange, S.K., Farren, N.J., Vaughan, A.R., Rose, R.A., Carslaw, D.C., 2019. Strong temperature dependence for light-duty diesel vehicle NO_x emissions. *Environ. Sci. Technol.* 53, 6587–6596. <https://doi.org/10.1021/acs.est.9b01024>.
- Heald, C.L., Kroll, J.H., Jimenez, J.L., Docherty, K.S., DeCarlo, P.F., Aiken, A.C., Chen, Q., Martin, S.T., Farmer, D.K., Artaxo, P., 2010. A simplified description of the evolution of organic aerosol composition in the atmosphere. *Geophys. Res. Lett.* 37 <https://doi.org/10.1029/2010GL042737>.
- Hu, W., Hu, M., Hu, W.W., Zheng, J., Chen, C., Wu, Y., Guo, S., 2017. Seasonal variations in high time-resolved chemical compositions, sources, and evolution of atmospheric submicron aerosols in the megacity Beijing. *Atmos. Chem. Phys.* 17, 9979–10000. <https://doi.org/10.5194/acp-17-9979-2017>.
- Hu, W., Zhou, H., Chen, W., Ye, Y., Pan, T., Wang, Y., Song, W., Zhang, H., Deng, W., Zhu, M., Wang, C., Wu, C., Ye, C., Wang, Z., Yuan, B., Huang, S., Shao, M., Peng, Z., Day, D.A., Campuzano-Jost, P., Lambe, A.T., Worsnop, D.R., Jimenez, J.L., Wang, X., 2022. Oxidation flow reactor results in a Chinese megacity emphasize the important contribution of S/IVOCs to ambient SOA formation. *Environ. Sci. Technol.* 56, 6880–6893. <https://doi.org/10.1021/acs.est.1c03155>.
- Huang, W., Saathoff, H., Shen, X., Ramisetty, R., Leisner, T., Mohr, C., 2019. Seasonal characteristics of organic aerosol chemical composition and volatility in Stuttgart, Germany. *Atmos. Chem. Phys.* 19, 11687–11700. <https://doi.org/10.5194/acp-19-11687-2019>.
- Jathar, S., Farina, S., Robinson, A., Adams, P., 2011. The influence of semi-volatile and reactive primary emissions on the abundance and properties of global organic aerosol. *Atmos. Chem. Phys. Discuss.* 11, 5493–5540. <https://doi.org/10.5194/acp-11-7727-2011>.
- Jathar, S.H., Miracolo, M.A., Tkacik, D.S., Donahue, N.M., Adams, P.J., Robinson, A.L., 2013. Secondary organic aerosol formation from photo-oxidation of unburned fuel: experimental results and implications for aerosol formation from combustion emissions. *Environ. Sci. Technol.* 47, 12886–12893. <https://doi.org/10.1021/es403445q>.
- Jimenez, J.L., Jayne, J.T., Shi, Q., Kolb, C.E., Worsnop, D.R., Yourshaw, I., Seinfeld, J.H., Flagan, R.C., Zhang, X., Smith, K.A., Morris, J.W., Davidovits, P., 2003. Ambient aerosol sampling using the Aerodyne aerosol mass spectrometer. *J. Geophys. Res. Atmos.* 108 <https://doi.org/10.1029/2001JD001213>.
- Kang, E., Root, M.J., Toohey, D.W., Brune, W.H., 2007. Introducing the concept of potential aerosol mass (PAM). *Atmos. Chem. Phys.* 7, 5727–5744. <https://doi.org/10.5194/acp-7-5727-2007>.
- Kang, S., Park, G., Park, T., Ban, J., Kim, K., Seo, Y., Choi, J., Seo, S., Choi, J., Bae, M.-S., Lee, T., 2020. Semi-continuous measurements of water-soluble organic carbon and ionic composition of PM2.5 in baengnyeong island during the 2016 KORUS-AQ (Korea-United States air quality study). *Asian J. Atmos. Environ.* 14 (3), 308–319. <https://doi.org/10.5572/ajae.2020.14.3.307>.
- Karavalakis, G., Short, D., Vu, D., Russell, R., Hajabaei, M., Asa-Awuku, A., Durbin, T. D., 2015. Evaluating the effects of aromatics content in gasoline on gaseous and particulate matter emissions from SI-PII and SIDII vehicles. *Environ. Sci. Technol.* 49, 7021–7031. <https://doi.org/10.1021/es5061726>.
- Karjalainen, P., Rönkkö, T., Simonen, P., Ntziachristos, L., Juuti, P., Timonen, H., Teinilä, K., Saarikoski, S., Saveljeff, H., Lauren, M., Happonen, M., Matilainen, P., Maunula, T., Nuottimäki, J., Keskinen, J., 2019. Strategies to diminish the emissions of particles and secondary aerosol formation from diesel engines. *Environ. Sci. Technol.* 53, 10408–10416. <https://doi.org/10.1021/acsc.est.9b04073>.
- Kim, H., Zhang, Q., Heo, J., 2018. Influence of intense secondary aerosol formation and long-range transport on aerosol chemistry and properties in the Seoul Metropolitan Area during spring time: results from KORUS-AQ. *Atmos. Chem. Phys.* 18, 7149–7168. <https://doi.org/10.5194/acp-18-7149-2018>.
- Kim, K., Park, G., Kang, S., Rahul, S., Song, J.-I., Choi, S., Park, I., Yu, D.-G., Kim, M.-B., Bae, M.-S., Jung, S., Chang, Y., Park, J., Jung, H.-J., Lim, Y.-J., Lee, T., 2021. Study of Inlet materials and measurement protocol for the real-time sampling of atmospheric Ammonia. *Asian J. Atmos. Environ.* 15 (4), 139–148. <https://doi.org/10.5572/ajae.2021.139>.
- Lambe, A., Onasch, T., Massoli, P., Croasdale, D., Wright, J., Ahern, A., Williams, L., Worsnop, D., Brune, W.H., Davidovits, P., 2011. Laboratory studies of the chemical composition and cloud condensation nuclei (CCN) activity of secondary organic aerosol (SOA) and oxidized primary organic aerosol (OPOA). *Atmos. Chem. Phys.* 11, 8913–8928. <https://doi.org/10.5194/acp-11-8913-2011>.
- Liao, K., Chen, Q., Liu, Y., Li, Y.J., Lambe, A.T., Zhu, T., Huang, R.-J., Zheng, Y., Cheng, X., Miao, R., Huang, G., Khuzestani, R.B., Jia, T., 2021. Secondary organic aerosol formation of fleet vehicle emissions in China: potential seasonality of spatial distributions. *Environ. Sci. Technol.* 55, 7276–7286. <https://doi.org/10.1021/acsc.est.0c08591>.
- Link, M.F., Kim, J., Park, G., Lee, T., Park, T., Babar, Z.B., Sung, K., Kim, P., Kang, S., Kim, J.S., Choi, Y., Son, J., Lim, H.-J., Farmer, D.K., 2017. Elevated production of NH₄NO₃ from the photochemical processing of vehicle exhaust: implications for air quality in the Seoul Metropolitan Region. *Atmos. Environ.* 156, 95–101. <https://doi.org/10.1016/j.atmosenv.2017.02.031>.
- Liu, H., Qi, L., Liang, C., Deng, F., Man, H., He, K., 2020. How aging process changes characteristics of vehicle emissions? A review. *Critical Reviews in Environ. Sci. Technol.* 50, 1796–1828. <https://doi.org/10.1080/10643389.2019.1669402>.
- Liu, J., Chu, B., Chen, T., Zhong, C., Liu, C., Ma, Q., Ma, J., Zhang, P., He, H., 2021. Secondary organic aerosol formation potential from ambient air in Beijing: effects of atmospheric oxidation capacity at different pollution levels. *Environ. Sci. Technol.* 55, 4565–4572. <https://doi.org/10.1021/acsc.est.1c00890>.
- Liu, T., Zhou, L., Liu, Q., Lee, B.P., Yao, D., Lu, H., Lyu, X., Guo, H., Chan, C.K., 2019. Secondary organic aerosol formation from urban roadside air in Hong Kong. *Environ. Sci. Technol.* 53, 3001–3009. <https://doi.org/10.1021/acsc.est.8b06587>.
- Lu, Q., Murphy, B.N., Qin, M., Adams, P.J., Zhao, Y., Pye, H.O.T., Efstathiou, C., Allen, C., Robinson, A.L., 2020. Simulation of organic aerosol formation during the CalNex study: updated mobile emissions and secondary organic aerosol parameterization for intermediate-volatility organic compounds. *Atmos. Chem. Phys.* 20, 4313–4332. <https://doi.org/10.5194/acp-20-4313-2020>.
- Ma, P., Zhang, P., Shu, J., Yang, B., Zhang, H., 2018. Characterization of secondary organic aerosol from photo-oxidation of gasoline exhaust and specific sources of major components. *Environ. Pollut.* 232, 65–72. <https://doi.org/10.1016/j.envpol.2017.09.018>.

- Mao, J., Ren, X., Brune, W., Olson, J., Crawford, J., Fried, A., Huey, L., Cohen, R., Heikes, B., Singh, H., 2009. Airborne measurement of OH reactivity during INTEX-B. *Atmos. Chem. Phys.* 9, 163–173. <https://doi.org/10.5194/acp-9-163-2009>.
- May, A.A., Presto, A.A., Hennigan, C.J., Nguyen, N.T., Gordon, T.D., Robinson, A.L., 2013. Gas-particle partitioning of primary organic aerosol emissions:(1) Gasoline vehicle exhaust. *Atmos. Environ.* 77, 128–139. <https://doi.org/10.1016/j.atmosenv.2013.04.060>.
- Middlebrook, A.M., Bahreini, R., Jimenez, J.L., Canagaratna, M.R., 2012. Evaluation of composition-dependent collection efficiencies for the Aerodyne aerosol mass spectrometer using field data. *Aerosol. Sci. Technol.* 46, 258–271. <https://doi.org/10.1080/02786826.2011.620041>.
- Ministry of Environment (MOE), 2017. National Air Pollutants Emission Report.
- Mitchell, L.E., Lin, J.C., Bowling, D.R., Pataki, D.E., Strong, C., Schauer, A.J., Bares, R., Bush, S.E., Stephens, B.B., Mendoza, D., Mallia, D., Holland, L., Gurney, K.R., Ehleringer, J.R., 2018. Long-term urban carbon dioxide observations reveal spatial and temporal dynamics related to urban characteristics and growth. *Proc. Natl. Acad. Sci. USA* 115, 2912. <https://doi.org/10.1073/pnas.1702393115>.
- Ng, N.L., Canagaratna, M.R., Jimenez, J.L., Chhabra, P.S., Seinfeld, J.H., Worsnop, D.R., 2011. Changes in organic aerosol composition with aging inferred from aerosol mass spectra. *Atmos. Chem. Phys.* 11, 6465–6474. <https://doi.org/10.5194/acp-11-6465-2011>.
- Park, G., Kim, K., Park, T., Kang, S., Ban, J., Choi, S., Yu, D.-G., Lee, S., Lim, Y., Kim, S., Mun, S., Woo, J.-H., Jeon, C.-S., Lee, T., 2021a. Primary and secondary aerosols in small passenger vehicle emissions: evaluation of engine technology, driving conditions, and regulatory standards. *Environ. Pollut.* 286, 117195 <https://doi.org/10.1016/j.envpol.2021.117195>.
- Park, C., Song, M., Park, G., Kim, K., Lee, T., Lee, S., Lee, J., Bae, M.-S., 2021b. Real-world vehicle emission rate of particle size distributions based on measurement of tunnel flow coefficient. *Appl. Sci.* 11, 794. <https://doi.org/10.3390/app11020794>.
- Park, G., Mun, S., Hong, H., Chung, T., Jung, S., Kim, S., Seo, S., Kim, J., Lee, J., Kim, K., Park, T., Kang, S., Ban, J., Yu, D.-G., Woo, J.-H., Lee, T., 2019. Characterization of emission factors concerning gasoline, LPG, and diesel vehicles via transient chassis-dynamometer tests. *Appl. Sci.* 9, 1573. <https://doi.org/10.3390/app9001573>.
- Park, T., Singh, R., Ban, J., Kim, K., Park, G., Kang, S., Choi, S., Song, J., Yu, D.-G., Bae, M.-S., Ahn, J., Jung, H.-J., Lim, Y.-J., Kim, H.W., Hwang, T.K., Choi, Y.J., Kim, S.-Y., Kim, H.S., Chang, Y.W., Shin, H.J., Lim, Y., Lee, J., Park, J., Choi, J., Lee, T., 2023. Seasonal and regional variations of atmospheric ammonia across the South Korean Peninsula. *Asian J. Atmos. Environ.* 17, 6. <https://doi.org/10.1007/s44273-023-00008-7>.
- Peng, Z., Jimenez, J.L., 2020. Radical chemistry in oxidation flow reactors for atmospheric chemistry research. *Chem. Soc. Rev.* 49, 2570–2616. <https://doi.org/10.1039/C9CS00766K>.
- Pieber, S.M., Kumar, N.K., Klein, F., Comte, P., Bhattu, D., Dommen, J., Bruns, E.A., Kılıç, D., El Haddad, I., Keller, A., Czerwinski, J., Heeb, N., Baltensperger, U., Slowik, J.G., Prévôt, A.S.H., 2018. Gas-phase composition and secondary organic aerosol formation from standard and particle filter-retrofitted gasoline direct injection vehicles investigated in a batch and flow reactor. *Atmos. Chem. Phys.* 18, 9929–9954. <https://doi.org/10.5194/acp-18-9929-2018>.
- Platt, S.M., El Haddad, I., Pieber, S.M., Zardini, A.A., Suarez-Bertoa, R., Clairotte, M., Daellenbach, K.R., Huang, R.J., Slowik, J.G., Hellebust, S., Temime-Roussel, B., Marchand, N., de Gouw, J., Jimenez, J.L., Hayes, P.L., Robinson, A.L., Baltensperger, U., Astorga, C., Prévôt, A.S.H., 2017. Gasoline cars produce more carbonaceous particulate matter than modern filter-equipped diesel cars. *Sci. Rep.* 7, 4926. <https://doi.org/10.1038/s41598-017-03714-9>.
- Robinson, A.L., Donahue, N.M., Shrivastava, M.K., Weitkamp, E.A., Sage, A.M., Grieshop, A.P., Lane, T.E., Pierce, J.R., Pandis, S.N., 2007. Rethinking organic aerosols: semi-volatile emissions and photochemical aging. *Science* 315, 1259–1262. <https://doi.org/10.1126/science.1133061>.
- Roth, P., Yang, J., Peng, W., Cocker, D.R., Durbin, T.D., Asa-Awuku, A., Karavalakis, G., 2020. Intermediate and high ethanol blends reduce secondary organic aerosol formation from gasoline direct injection vehicles. *Atmos. Environ.* 220, 117064 <https://doi.org/10.1016/j.atmosenv.2019.117064>.
- Rowe, J.P., Lambe, A.T., Brune, W.H., 2020. Technical Note: effect of varying the $\lambda = 185$ and 254 nm photon flux ratio on radical generation in oxidation flow reactors. *Atmos. Chem. Phys.* 20, 13417–13424. <https://doi.org/10.5194/acp-20-13417-2020>.
- Saha, P.K., Reece, S.M., Grieshop, A.P., 2018a. Seasonally varying secondary organic aerosol formation from in-situ oxidation of near-highway air. *Environ. Sci. Technol.* 52, 7192–7202. <https://doi.org/10.1021/acs.est.8b01134>.
- Saha, P.K., Khlystov, A., Snyder, M.G., Grieshop, A.P., 2018b. Characterization of air pollutant concentrations, fleet emission factors, and dispersion near a North Carolina interstate freeway across two seasons. *Atmos. Environ.* 177, 143–153. <https://doi.org/10.1016/j.atmosenv.2018.01.019>.
- Saliba, G., Saleh, R., Zhao, Y., Presto, A.A., Lambe, A.T., Frodin, B., Sardar, S., Maldonado, H., Maddox, C., May, A.A., 2017. Comparison of gasoline direct-injection (GDI) and port fuel injection (PFI) vehicle emissions: emission certification standards, cold-start, secondary organic aerosol formation potential, and potential climate impacts. *Environ. Sci. Technol.* 51, 6542–6552. <https://doi.org/10.1021/acs.est.6b06509>.
- Shah, R.U., Coggon, M.M., Gkatzelis, G.I., McDonald, B.C., Tasoglou, A., Huber, H., Gilman, J., Warneke, C., Robinson, A.L., Presto, A.A., 2020. Urban oxidation flow reactor measurements reveal significant secondary organic aerosol contributions from volatile emissions of emerging importance. *Environ. Sci. Technol.* 54, 714–725. <https://doi.org/10.1021/acs.est.9b06531>.
- Simonen, P., Kalliokoski, J., Karjalainen, P., Rönkkö, T., Timonen, H., Saarikoski, S., Aurela, M., Bloss, M., Triantafyllopoulos, G., Kontses, A., Amanatidis, S., Dimaratos, A., Samaras, Z., Keskinen, J., Dal Maso, M., Ntzachristos, L., 2019. Characterization of laboratory and real driving emissions of individual Euro 6 light-duty vehicles – fresh particles and secondary aerosol formation. *Environ. Pollut.* 255, 113175 <https://doi.org/10.1016/j.envpol.2019.113175>.
- Suarez-Bertoa, R., Zardini, A.A., Astorga, C., 2014. Ammonia exhaust emissions from spark ignition vehicles over the New European Driving Cycle. *Atmos. Environ.* 97, 43–53. <https://doi.org/10.1016/j.atmosenv.2014.07.050>.
- Sydbom, A., Blomberg, A., Parnia, S., Stenfors, N., Sandstrom, T., Dahlén, S.-E., 2001. Health effects of diesel exhaust emissions. *Eur. Respir. J.* 17, 733–746.
- Tkacik, D.S., Lambe, A.T., Jathar, S., Li, X., Presto, A.A., Zhao, Y., Blake, D., Meinardi, S., Jayne, J.T., Croteau, P.L., Robinson, A.L., 2014. Secondary organic aerosol formation from in-use motor vehicle emissions using a potential aerosol mass reactor. *Environ. Sci. Technol.* 48, 11235–11242. <https://doi.org/10.1021/es502239v>.
- Turner, A.J., Kim, J., Fitzmaurice, H., Newman, C., Worthington, K., Chan, K., Woolridge, P.J., Köehler, P., Frankenberger, C., Cohen, R.C., 2020. Observed impacts of COVID-19 on urban CO₂ emissions. *Geophys. Res. Lett.* 47, e2020GL090037 <https://doi.org/10.1029/2020GL090037>.
- Walters, W.W., Song, L., Chai, J., Fang, Y., Colombi, N., Hastings, M.G., 2020. Characterizing the spatiotemporal nitrogen stable isotopic composition of ammonia in vehicle plumes. *Atmos. Chem. Phys.* 20, 11551–11567. <https://doi.org/10.5194/acp-20-11551-2020>.
- Wang, J.M., Jeong, C.-H., Zimmerman, N., Healy, R.M., Evans, G.J., 2018. Real world vehicle fleet emission factors: seasonal and diurnal variations in traffic related air pollutants. *Atmos. Environ.* 184, 77–86. <https://doi.org/10.1016/j.atmosenv.2018.04.015>.
- Wang, X., Ge, Y., Gong, H., Yang, Z., Tan, J., Hao, L., Su, S., 2019a. Ammonia emissions from China-6 compliant gasoline vehicles tested over the WLTC. *Atmos. Environ.* 199, 136–142. <https://doi.org/10.1016/j.atmosenv.2018.11.027>.
- Wang, Q., Zhang, Q., Ma, Z., Ge, B., Xie, C., Zhou, W., Zhao, J., Xu, W., Du, W., Fu, P., Lee, J., Nemitz, E., Cowan, N., Mullinger, N., Cheng, X., Zhou, L., Yue, S., Wang, Z., Sun, Y., 2019b. Temporal characteristics and vertical distribution of atmospheric ammonia and ammonium in winter in Beijing. *Sci. Total Environ.* 681, 226–234. <https://doi.org/10.1016/j.scitotenv.2019.05.137>.
- Wichmann, H.E., 2007. Diesel exhaust particles. *Inhal. Toxicol.* 19, 241–244. <https://doi.org/10.1080/08958370701498075>.
- Zhang, S., Niu, T., Wu, Y., Zhang, K.M., Wallington, T.J., Xie, Q., Wu, X., Xu, H., 2018. Fine-grained vehicle emission management using intelligent transportation system data. *Environ. Pollut.* 241, 1027–1037. <https://doi.org/10.1016/j.envpol.2018.06.016>.
- Zhao, Y., Lambe, A.T., Saleh, R., Saliba, G., Robinson, A.L., 2018. Secondary organic aerosol production from gasoline vehicle exhaust: effects of engine technology, cold start, and emission certification standard. *Environ. Sci. Technol.* <https://doi.org/10.1021/acs.est.7b05045>.
- Zhao, Y., Nguyen, N.T., Presto, A.A., Hennigan, C.J., May, A.A., Robinson, A.L., 2015. Intermediate volatility organic compound emissions from on-road diesel vehicles: chemical composition, emission factors, and estimated secondary organic aerosol production. *Environ. Sci. Technol.* 49, 11516–11526. <https://doi.org/10.1021/acs.est.5b02841>.
- Zhao, Y., Nguyen, N.T., Presto, A.A., Hennigan, C.J., May, A.A., Robinson, A.L., 2016. Intermediate volatility organic compound emissions from on-road gasoline vehicles and small off-road gasoline engines. *Environ. Sci. Technol.* 50, 4554–4563. <https://doi.org/10.1021/acs.est.5b02427>.
- Zhao, Y., Saleh, R., Saliba, G., Presto, A.A., Gordon, T.D., Drozd, G.T., Goldstein, A.H., Donahue, N.M., Robinson, A.L., 2017. Reducing secondary organic aerosol formation from gasoline vehicle exhaust. *Proc. Natl. Acad. Sci. U. S. A.* 114, 6984–6989. <https://doi.org/10.1073/pnas.1620911114>.
- Zhou, W., Gao, M., He, Y., Wang, Q., Xie, C., Xu, W., Zhao, J., Du, W., Qiu, Y., Lei, L., 2019a. Response of aerosol chemistry to clean air action in Beijing, China: insights from two-year ACSM measurements and model simulations. *Environ. Pollut.* 255, 113345 <https://doi.org/10.1016/j.envpol.2019.113345>.
- Zhou, C., Zhou, H., Holsen, T.M., Hopke, P.K., Edgerton, E.S., Schwab, J.J., 2019b. Ambient ammonia concentrations across New York state. *J. Geophys. Res. Atmos.* 124, 8287–8302. <https://doi.org/10.1029/2019JD030380>.
- Zhou, W., Xu, W., Kim, H., Zhang, Q., Fu, P., Worsnop, D.R., Sun, Y., 2020. A review of aerosol chemistry in Asia: insights from aerosol mass spectrometer measurements. *Environ. Sci. Process. Impacts* 22, 1616–1653. <https://doi.org/10.1039/D0EM00212G>.
- Żółtowski, A., Gis, W., 2021. Ammonia emissions in SI engines fueled with LPG. *Energy* 14, 691. <https://doi.org/10.3390/en14030691>.